SCIENTIFIC REPORTS

OPEN

Fast Ionic Diffusion-Enabled Nanoflake Electrode by Spontaneous Electrochemical Pre-Intercalation for High-Performance Supercapacitor

Liqiang Mai[1], Han Li[1], Yunlong Zhao[1], Lin Xu[1,2], Xu Xu[1], Yanzhu Luo[1], Zhengfei Zhang[1], Wang Ke[1], Chaojiang Niu[1] & Qingjie Zhang[1]

[1]State Key Laboratory of Advanced Technology for Materials Synthesis and Processing, WUT-Harvard Joint Nano Key Laboratory, Wuhan University of Technology, Wuhan 430070, China, [2]Department of Chemistry and Chemical Biology, Harvard University, Cambridge, Massachusetts 02138.

Layered intercalation compounds Na_xMnO_2 (x = 0.7 and 0.91) nanoflakes have been prepared directly through wet electrochemical process with Na^+ ions intercalated into MnO_2 interlayers spontaneously. The as-prepared Na_xMnO_2 nanoflake based supercapacitors exhibit faster ionic diffusion with enhanced redox peaks, tenfold-higher energy densities up to 110 $Wh \cdot kg^{-1}$ and higher capacitances over 1000 $F \cdot g^{-1}$ in aqueous sodium system compared with traditional MnO_2 supercapacitors. Due to the free-standing electrode structure and suitable crystal structure, Na_xMnO_2 nanoflake electrodes also maintain outstanding electrochemical stability with capacitance retention up to 99.9% after 1000 cycles. Besides, pre-intercalation effect is further studied to explain this enhanced electrochemical performance. This study indicates that the suitable pre-intercalation is effective to improve the diffusion of electrolyte cations and other electrochemical performance for layered oxides, and suggests that the as-obtained nanoflakes are promising materials to achieve the hybridization of both high energy and power density for advanced supercapacitors.

Supercapacitors, with high power density and long operating life, are expected to provide potential access to bridge the gap between batteries and conventional capacitors[1–10]. However, one of the key challenges for supercapacitors to achieve wide application is increasing their energy density[1,3].

As one of the most promising pseudocapacitive electrode materials, MnO_2 has a relatively high energy density because of its high reversible redox reaction. For example, it can exhibit a redox reaction in sodium electrolyte system based on the following charge storage mechanism (Equations (1))[3,11]:

$$MnO_2 + xH^+ + yNa^+ + (x+y)e^- \leftrightarrow MnOOH_xNa_y \qquad (1)$$

Here are three rate-controlling steps involved in this reaction during the Mn III/IV oxidation state change: (i) Adsorption of electrochemically active ions on the surface of electrode; (ii) Electronic transfer drived by current collector; (iii) Na^+ (or H^+) ions diffusion and intercalation/deintercalation.

For rate-controlling step (i), large active surface area is important to enhance the ionic adsorption. For rate-controlling step (ii), we can electrodeposit MnO_2 on the nickel foam to obtain the continuous electronic transfer path. While for rate-controlling step (iii), it is important to improve the long-distance ionic diffusion ability from electrolyte to the solid phase, which is very difficult for traditional MnO_2[12,13]. To solve this problem, researchers reduce the diffusion resistance in the solid phase by decreasing the size and shortening the diffusion paths[13–16], facilitated the ionic diffusion between MnO_2 and electrolyte by constructing an interconnected porous system[10,17–22], or even loading very small quantity of active mass to achieve high capacitance. However, those strategies can improve the diffusion and intercalation/deintercalation only on the surface or the interface, the low ionic diffusion inside the solid phase is still unsolved fundamentally.

Recently, sodium-intercalation layered compounds Na_xMO_2 (M = Mn[23–25], Co[26,27], V[28], etc) were synthesized to deliver high electrochemical activity of Na^+ ions due to their interesting crystal structure. Among them, $Na_{0.7}MnO_2$ and $Na_{0.91}MnO_2$ are electrochemically attractive due to high sodium cationic distribution and

layered intercalation structure[23]. However, all those reported Na$_x$MnO$_2$ were synthesized by high-temperature solid reactions, and that will greatly increase the products' practical energy consumption, complexity, and crystal size, which is not suitable for supercapacitors.

In our previous work, we have successfully intercalated metallic ions to improve electrochemical performance for energy storage by secondary hydrothermal process[29]. Here, to improve the diffusion performance of Na$^+$ ions in MnO$_2$ solid phase, we used a one-step electrodeposition technique, based on the atomic-level control of material composition[30], to rationally obtain electrochemically active layered Na$_x$MnO$_2$ (x $\geq$ 0.7) phases (Figure 1a and b). Na$^+$ was intercalated spontaneously in MnO$_2$ crystal interlayers without any rigorous condition such as thermal treatment or complex solid reactions. The as-obtained nanoflake electrode exhibited good Na$^+$ diffusion behaviors and excellent electrochemical performance in 1 M Na$_2$SO$_4$ solution even when the loading mass was as large as 2.25 mg·cm^{-2}. Such good results demonstrate that our rational, facile, mild and controllable method to produce Na$_x$MnO$_2$ naomaterials is promising for fabrication of high-level energy devices for large-scale practical application[31–33].

Results

According to XRD patterns (Figure 1a), the phase of electrodeposited products changes with deposition time. The Na$_{0.7}$MnO$_2$ (JCPDS No. 00-027-0752) is deposited in the initial 20 min. Then Na$_{0.91}$MnO$_2$ (JCPDS No. 00-038-0965) and MnO$_2$ (JCPDS No. 00-011-0055) are produced with more Na$^+$ intercalated into the layer structure during 20–100 min. With time extended to 200 min, the Na$_{0.7}$MnO$_2$ phase changes to Na$_{0.91}$MnO$_2$. The Atomic Adsorption Spectrum (AAS) was measured to demonstrate the ratio of Na and Mn (Supplementary information, Table 1), and the analysis is identical with the XRD results. Energy dispersive X-ray spectrometry (EDS) mapping (Supplementary information, Figure S1a) further confirms that Na, Mn and O atoms are homogeneously distributed in all of the nanoflakes. Besides, XRD of hydrothermally synthesized α-MnO$_2$ (JCPDS No. 00-044-0141) controlled nanowires is also given for comparison with Na$_x$MnO$_2$.

Typical scanning electron microscopic (SEM) images (Figure 2a) show that excessive agglomerations are prevented effectively. A loose and interconnected nanoflake structure with large surface areas is obtained and these nanoflakes were closely attached to nickel surface (electron path), forming good electrochemical connection.
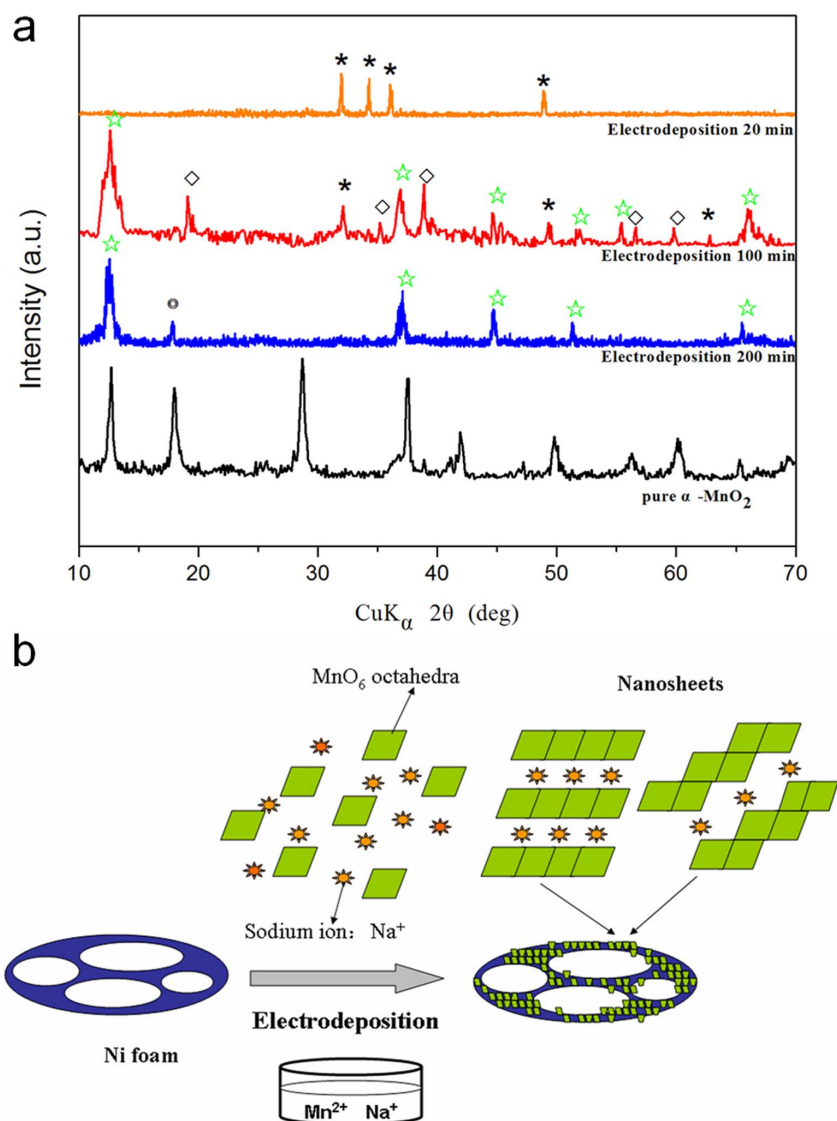

Figure 1 | Phase characterization and schematic Na$^+$ intercalation mechanism of pre-intercalated MnO$_2$ nanoflake electrodes. (a) Typical XRD of Na$_x$MnO$_2$/MnO$_2$ with electrodeposition time: 20 min (yellow line); 100 min (red line); 200 min (blue line). Symbols *, ☆ respectively represent Na$_{0.7}$MnO$_2$, Na$_{0.91}$MnO$_2$, and ◇, ◎ represent MnO$_2$. (b) Proposed mechanism for intercalation of Na$^+$ ions into MnO$_2$ interlayers.
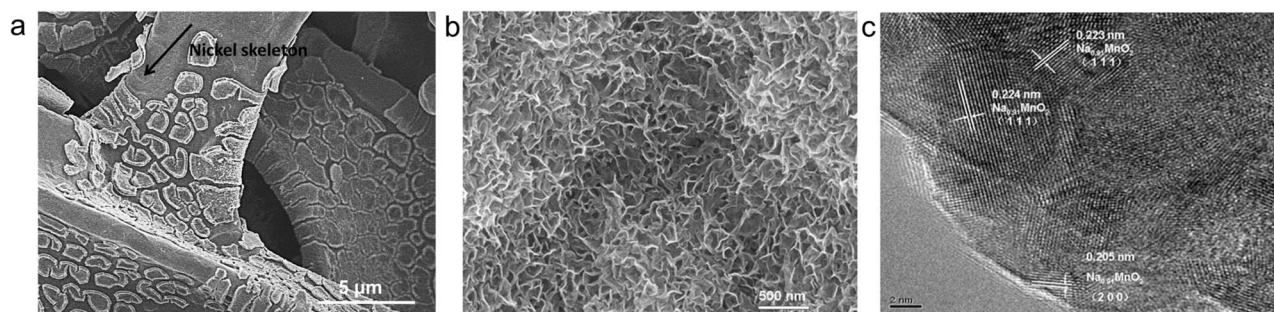
Figure 2 | Morphology characterization of pre-intercalated MnO₂ nanoflake electrodes. (a, b) SEM images of the electrodeposited uniform nanoflakes on the nickel skeleton with average thickness of 15–20 nm. (c) HRTEM image of Na_xMnO_2/MnO_2 nanoflakes after 200 min electrodeposition.

Significantly, these ultrathin nanoflakes with large surface area are beneficial for the adsorption of the electroactive ions and contact with electrolyte. As a result, diffusion and intercalation/deintercalation of Na^+ ions have been facilitated by the nanoflake morphology. The high-resolution transmission electron microscopic (HRTEM) investigation (Figure 2b, Supplementary Figure S1b) reveals polycrystalline structure of the nanoflake. By comparing interplanar distances measured from HRTEM with the theoretical value, the existence of $Na_{0.91}MnO_2$ and $Na_{0.7}MnO_2$ is confirmed, consistent with the results from XRD crystal analysis.

Cyclic Voltammetry tests (CVs) were performed to identify the charge storage mechanism in 1 M Na_2SO_4. According to Figure 3a, obviously a pair of redox peaks appear in the CV curve of Na_xMnO_2/MnO_2 electrode while no redox peaks are found in the CV curve of α-MnO_2 sample. It is interesting that according to many reported work, no such peaks related to redox reaction of MnO_2 have been ever observed with respect to α-MnO_2[34–36], β-MnO_2[36], γ-MnO_2[36], δ-MnO_2[36], ε-MnO_2[10,34], nanocrystalline MnO_2[20], MnO_2 composite electrodes[17,18] and so on when the same Na_2SO_4 is used as electrolyte. The occurrence of redox peaks implies that the charge storage mechanism is mainly based on redox reaction. The potential difference between the anodic and cathodic peak is about 0.06 V, representing a highly reversible intercalation/deintercalation during the whole electrochemical process.

According to Figure 3b, with the increase of the scan rate, the redox current gets larger, the anodic peak shifts towards positive potential and the cathodic peak shifts towards negative potential. And the inset shows that, the specific capacitance of the electrode increase as the scan rate decrease from 500 to 1 mV·s⁻¹. As observed in both Figure 3a inset and Figure 4a inset b, it is interesting that the slopes of potential-time curves change with inflexion points arising between 0.4 and 0.6 V during charge and discharge process, representing the occurrence of redox reaction, which is greatly consistent with the appearance of redox peaks in CV.

According to the galvanostatic charge–discharge curves of electrodes in 1 M Na_2SO_4 at room temperature, average capacitance during the whole discharge process has been calculated from Equation (2):

$$C_s = \frac{it}{VS} \qquad (2)$$

Where i (A) is the current density applied in charge/discharge, t (s) is the time elapsed in the discharge cycle, S (cm²) is the geometric area of the active electrode and V (V) is the voltage interval of the discharge.

The areal capacitances are estimated from discharge curves at different current densities from 0.17 to 30 mA·cm⁻² (Figure 4a). The capacitance contributed by bare nickel foam can be negligible (Supplementary Figure S4). All the capacitance curves show that the areal capacitances increase as the areal current densities decrease. At the lowest current densities 0.17 mA·cm⁻², the obtained areal capacitance for 200, 100, 20 min reach up to maximum 2.08, 1.46, 0.25 F·cm⁻², respectively, which are comparable to as-reported high capacitance[17,37,38]. Even at the largest current density 30 mA·cm⁻² which produces the lowest areal capacitance, the areal capacitance of 10–30 mF·cm⁻² in our work is still much higher than that of reported MnO_2 film[14,17,18,20]. When compressed at 10 MPa, the nickel foam-supported Na_xMnO_2/MnO_2 electrode is paper-like with a thickness of merely 50 μm (Supplementary Figure S5 inset), much thinner than other supporters such as textiles[17], sponge[10], ITO glasses[18], PET[20], bringing a higher volumetric capacitances over 100 F·cm⁻³ (Supplementary Figure S5) based on volume of the total electrode.

Figure 4b shows that, based on loading mass of 2.25, 1.17, 0.23 mg·cm⁻² for 200, 100, 20 min, the obtained high gravimetric capacitance of 903, 1237, 1058 F·g⁻¹ at 0.17 mA·cm⁻² can be correspondingly normalized to 205, 280, 240 mAh·g⁻¹ (Figure 4b inset). The electrode with 100 min deposition exhibits the larger gravimetric capacitance than that with 200 min deposition. According to current understanding, with the increase of active mass, the gravimetric capacitance decreases, due to large internal resistance (Supplementary information, Table 3) and difficult ionic diffusion.

Considering that the highest areal capacitance is obtained when the deposition time is 200 min, we further investigated its cycling performance, as shown in Figure 5. Typically such electrode exhibits both high areal capacitance of 350 mF·cm⁻² at 5 mA·cm⁻² (2.2 A·g⁻¹) and ultra-high reversibility with excellent capacitance retention of 99.9% after 1,000 cycles, and 95.2% after 5000 cycles (Supplementary Figure S6), which represents long life in practical applications because of good structural and electrochemical stability of Na_xMnO_2/MnO_2 electrodes.

We calculated the half cell (3-electrode) energy density and power density of as-electrodeposited electrodes according to the Equations (3) and (4) as follows:

$$E = \frac{CV^2}{2M} \qquad (3)$$

$$P = \frac{V^2}{4RM} \qquad (4)$$

C (F·cm⁻²) represents the areal capacitance; V (V) is the voltage window; R (Ω·cm⁻²) is the areal internal resistance (Supplementary information, Table 3). According to the Ragone Plot in Figure 6, ultrahigh power densities (based on active material) are obtained from 64.6 to 836.9 KW·kg⁻¹ at different current densities, which are at least tenfold higher than those of conventional MnO_2 supercapacitors, resulting from a perfect ionic and electronic mobility during the electrochemical process. Besides, high energy density up to 110 Wh·kg⁻¹ (half cell, based on active material; or 55 Wh·kg⁻¹ for full cell), is also comparable to the reported values[20].
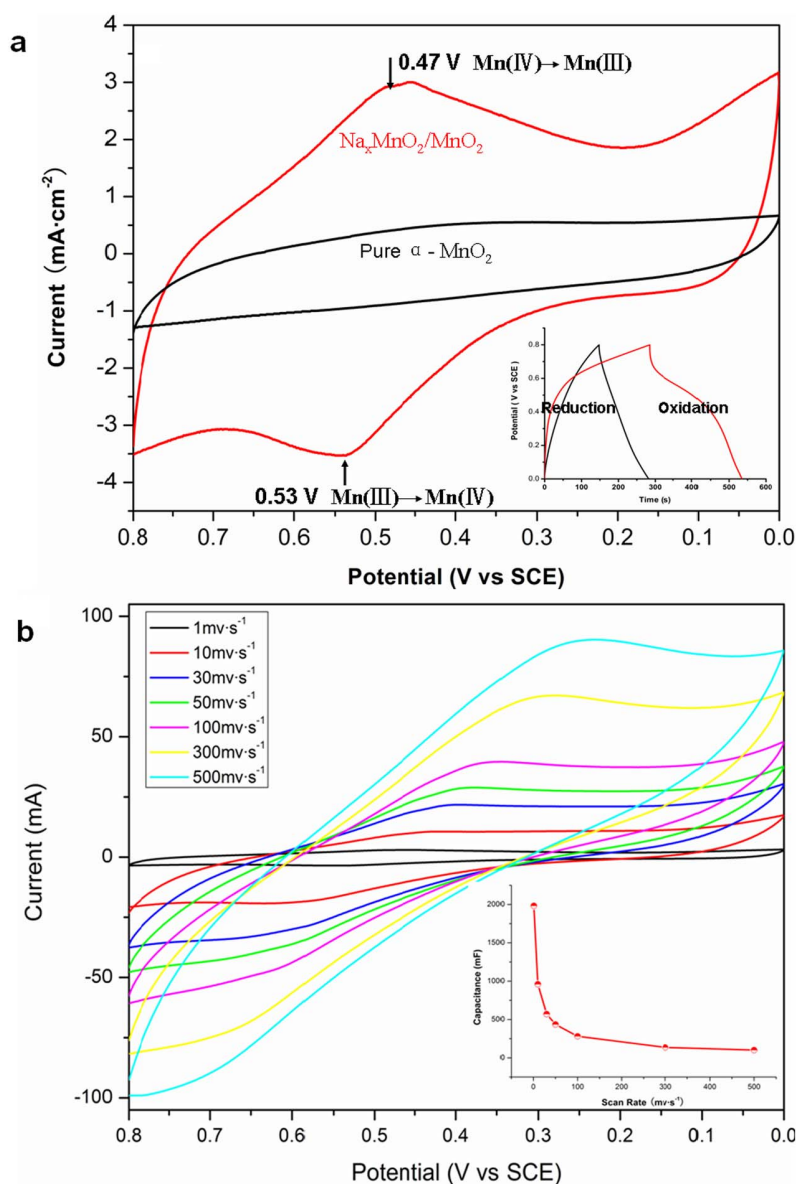
Figure 3 | Cyclic voltammograms of Na$_x$MnO$_2$/MnO$_2$ electrodes in 1M Na$_2$SO$_4$. (a) Cyclic voltammograms of Na$_x$MnO$_2$/MnO$_2$ (electrodeposition time: 200 min) and pure α-MnO$_2$ at scan rate of 1 mV·s^{-1}; inset: comparison of discharge process between Na$_x$MnO$_2$/MnO$_2$ and α-MnO$_2$ at current density of 1 mA·cm^{-2}. (b) Cyclic voltammograms of Na$_x$MnO$_2$/MnO$_2$ (electrodeposition time: 200 min) at different scan rates from 1 mV·s^{-1} to 500 mV·s^{-1}; inset: the capacitance calculated by CV curve at corresponding scan rate, potential window: 0–0.8 V (vs. SCE).

Discussion

As reported, the layered intercalation compounds Na$_x$MnO$_2$ were conventionally prepared by high-temperature solid reaction[23–25,34]. Here, the sodium pre-intercalation Na$_x$MnO$_2$ (x = 0.7 or 0.91) was firstly synthesized by electrodeposition method, a kind of wet electrochemical methods. The probable formation mechanism of Na$_x$MnO$_2$ is shown in Figure 1b. During the electrodeposition process, the MnO$_2$, sharing [MnO$_6$] octahedra edge with each other, is firstly deposited on the Ni skeleton with a series of successive electrochemical redox reaction, then the nanoflakes formed. In particular, under the large concentration of sodium ions (Na$^+$:Mn^{2+} = 100 : 1), the as-synthesized layered MnO$_2$ simultaneously enables sodium ions to intercalate into its interlayers, according to the electrostatic balance and energy minimization theory. The final sodium distributive layered Na$_x$MnO$_2$ (x = 0.7) is obtained. With longer deposition time, more sodium ions are allowed to enter into the interlayers of MnO$_2$. Consequently, higher sodium content is

obtained in the final electrodeposited product of Na$_x$MnO$_2$ (x = 0.91), confirmed by XRD results. The finding of hybrid MnO$_2$ phase in the final product is consistent with previous reports of electrodeposition[10,17,19–21,39–41], which indicates simultaneous formation of MnO$_2$ with spontaneous intercalation of Na$^+$ ions in MnO$_2$ interlayers. The XRD results further confirm that the intercalation of Na$^+$ ions into MnO$_2$ interlayers is time dependent with phase transition from Na$_{0.7}$MnO$_2$ to Na$_{0.91}$MnO$_2$.

A pre-intercalation effect is proposed to explain the excellent electrochemical performance of Na$_x$MnO$_2$/MnO$_2$ in this work. For traditional hydrothermally synthesized α-MnO$_2$ in Na$_2$SO$_4$ electrolyte, it exhibits a pseudo-constant rate over the entire CV tests, due to the difficult and long distance Na$^+$ diffusion in the MnO$_2$ interlayers, responding to rectangular shape without redox peaks in the CV curve. However, the observed redox peaks in Na$_x$MnO$_2$ electrode are attributed to a pre-intercalation effect. On one hand, this kind of intercalation of Na$^+$ in MnO$_2$ nanoflackes can be regarded as a
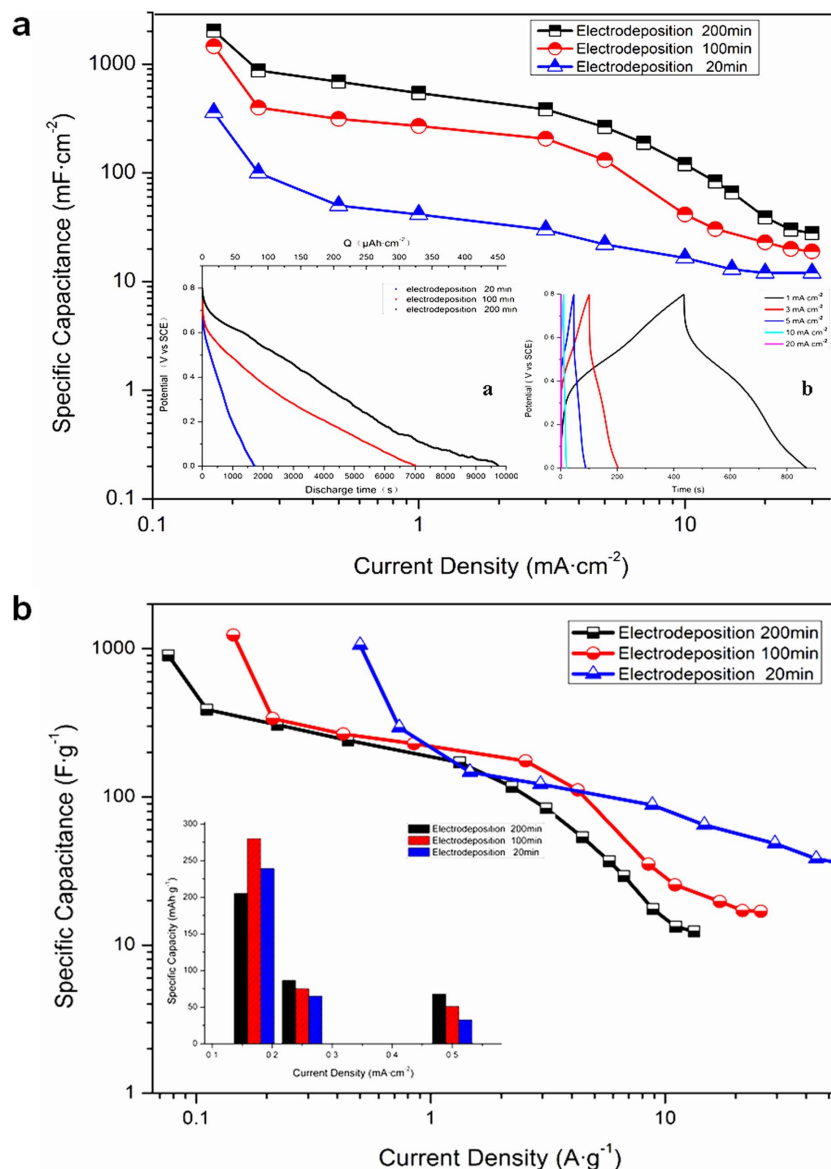
Figure 4 | Areal and gravimetric capacitance of pre-intercalated MnO₂ with different deposition time. (a) Areal capacitance for different deposition time (20 min, 100 min, 200 min) at different current densities ranged from 0.17 to 30 mA·cm⁻², current densities from left to right: 0.17, 0.25, 0.5, 1, 3, 5, 7, 10, 13, 15, 20, 25, 30 mA·cm⁻²; inset a, galvanostatic discharge profiles of each electrode at 0.17 mA·cm⁻²; inset b, galvanostatic charge and discharge profiles of electrode after electrodeposition of 200 min at current densities from 1 to 20 mA·cm⁻². (b) Gravimetric capacitance normalized by given loading mass of different deposition time; inset: capacities normalized to mAh·g⁻¹ at current densities 0.17, 0.25 and 0.5 mA·cm⁻².

pre-intercalation process of electrolyte cations during the electro-deposition process. On the other hand, such pre-intercalation facilitates the subsequent electrochemical ion diffusion, intercalation/deintercalation and transport process, leading to the redox process of Mn between Mn (IV) and Mn (III). The as-observed redox peaks in CV curves at 0.4–0.6 V (vs. SCE) are exactly identical with the theoretical transformation potential between Mn (IV) and Mn (III), according to the Mn Pourbaix diagram (Supplementary Figure S7). Moreover, with the increase of the scan rate up to 500 mV·s⁻¹, the kinetics of Faradic redox reactions and the high rate of electronic and ionic transport are able to successfully occur, which indicates the Na$_x$MnO₂/MnO₂ ultrathin nanoflakes on Ni electrode allow easy and efficient access of electrons and ions. The sodium ion diffusion coefficient (D$_{Na}^+$) of Na$_x$MnO₂/MnO₂ was calculated to testify the facilitated Na$^+$ diffusion by pre-intercalation, according to the Randles-Sevick equation[42,43]. The D$_{Na}^+$ here is up to 3.07×10^{-6} cm²·S⁻¹ (Supplementary information, Calculation 1), which is three orders of magnitude larger than that of currently reported compounds[23], revealing the fast diffusion of Na$^+$ is accelerated by pre-intercalation. Besides, the ultrahigh power density and battery level energy density (Figure 6) also reveal a much better ionic and electronic mobility during the electrochemical process than that of traditional MnO₂. Such results can prove that the as-obtained Na$_x$MnO₂ phases exhibit high electrochemical activity of Na$^+$ to enhance the redox process of Mn (IV)/Mn (III) in Na₂SO₄ electrolyte.

To further identify the pre-intercalation effect, we have compared the electrochemical performance of M$_x$MnO₂ (M:Na$^+$ or Li$^+$) in different electrolytic systems (Na₂SO₄ or Li₂SO₄) (Supplementary discussion). As a result, in Na₂SO₄ electrolyte, better electrochemical performance is obtained when Na$^+$ instead of Li$^+$ intercalated in MnO₂ interlayers (Supplementary Figure S3). Such result reveals that the pre-intercalation effect of electrolyte cations in active mass is greatly related to the subsequent electrochemical performance.
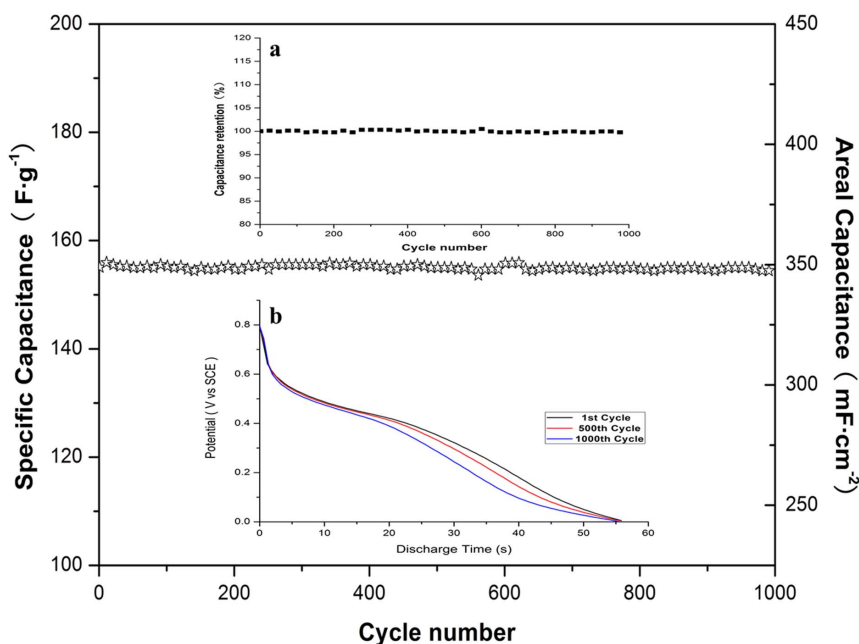
Figure 5 | Cycling performance of Na$_x$MnO$_2$/MnO$_2$ electrode at current density of 5 mA·cm^{-2} (2.2 A·g^{-1}). Inset: (a) the capacity retention during 1000 cycles and (b) discharge profiles with respect to initial cycle (black line), 500th cycle (red line), 1000th cycle (blue line).

In summary, sodium ions have been spontaneously intercalated into MnO$_2$ interlayers with two layered Na$_{0.91}$MnO$_2$ and Na$_{0.7}$MnO$_2$ phases obtained by electrodeposition. Such Na$_x$MnO$_2$/MnO$_2$ electrode exhibits excellent supercapacitor performance especially in Na$^+$ electrolytic system, delivering both ultrahigh power density and energy density up to 110 Wh·kg^{-1} (half cell based on active materials). These electrodes also maintain outstanding electrochemical stability with capacitance retention up to 99.9% after 1000 cycles. According to the calculation and electrochemical comparison, the Na$^+$ diffusion of Na$_x$MnO$_2$/MnO$_2$ electrode is confirmed to be greatly facilitated. The pre-intercalation effect was proposed to explain the excellent electrochemical behaviors of Na$_x$MnO$_2$/MnO$_2$. This electrochemical pre-intercalation proves to be an effective route to enhance the diffusion of electrolyte cations for layered oxides, and the as-obtained Na$_x$MnO$_2$/MnO$_2$ ($x = 0.7$ or 0.91) nanoflakes are promising materials for supercapacitors to achieve the hybridization of both high energy and power densities for large-scale industrial applications.
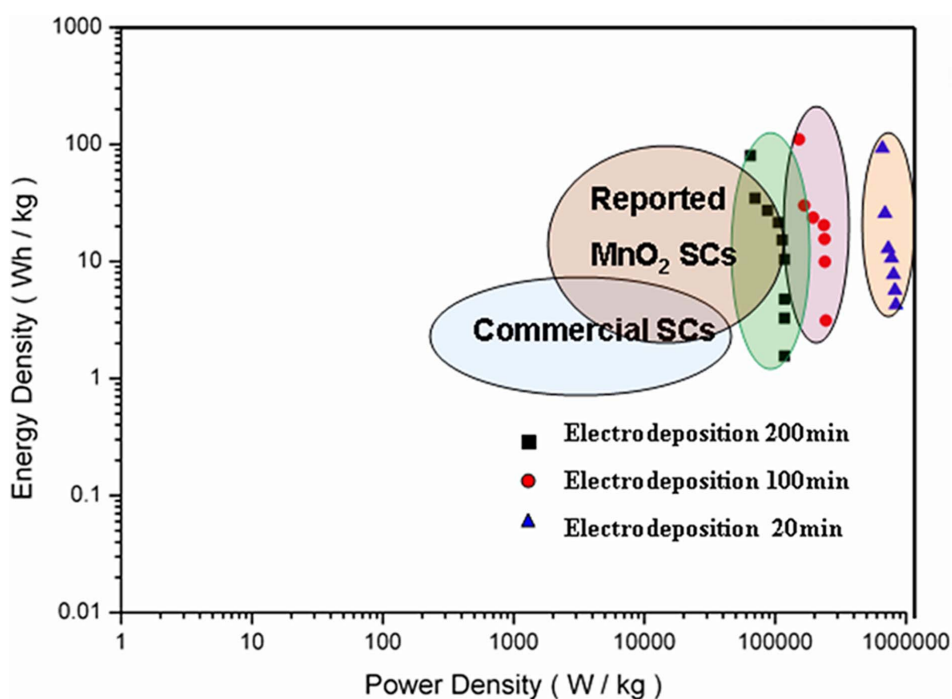

Figure 6 | The Ragone Plot of electrodeposited electrode. Energy density and power density with different deposition time (20, 100, 200 min) at different currents from 0.17 to 20 mA·cm^{-2}. The area for reported MnO$_2$ supercapacitors and commercial supercapacitors are plotted and modified by reference to Lang's supporting information[20].

Methods

Modified electrodeposition for Na$_x$MnO$_2$. Currently, solutions for electrodeposited MnO$_2$ were reported to be consisted of Mn (II) compounds such as MnSO$_4$ or Mn(CH$_3$COO)$_2$ as manganese sources[17,19–21,39–41], and 0.1–0.2 M Na$_2$SO$_4$ as additives[17,20,41]. In our work, 0.02 M Mn(CH$_3$COO)$_2$ and 1 M Na$_2$SO$_4$ were used as mother solution, which provided a much larger concentration ratio (Na$^+$:Mn^{2+} = 100 : 1), so as to conduct the intercalation of Na$^+$ ions in MnO$_2$ layers by electrodeposition.

Sodium intercalation was carried out by anodically galvanostatic electrodeposition, using a three-electrode configuration with nickel foam (1 × 1 cm) as working electrode, Pt as counter electrode and Ag/AgCl (saturated KCl) as reference electrode. Here nickel foam was used to provide support for electrodeposited Na$_x$MnO$_2$ and good electric conductivity for the total electrode. The deposition was carried out by Autolab Potentiostat Galvanostat. As-electrodeposited Na$_x$MnO$_2$/MnO$_2$ nanoflakes were obtained at current density of 350–500 μA·cm^{-2} for 20, 100, 200 min with loading mass of 0.23, 1.17, 2.25 mg·cm^{-2}, respectively Large nickel foams with area of 5–10 cm^2 were used to identify the average loading mass by microbalance before and after the electrodeposition in a fully dried condition. As-electrodeposited electrode was naturally dried under 25°C to prevent the detachment of active materials from nickel foam. Loading mass with respect to each electrode was identified by over three times. Li$_x$Mn$_2$O$_4$ was also prepared for comparison in electrochemistry with Na$^+$ pre-intercalated electrode. Method and process were the same for pre-intercalation of Li$^+$ ions into MnO$_2$ layers, with only Na$_2$SO$_4$ (1 M) solution replaced by Li$_2$SO$_4$ (1 M) solution. Pure α-MnO$_2$ was synthesized by hydrothermal method with 2 mmol KMnO$_4$ and 3 mmol MnSO$_4$ in 80 ml deionized water at 160°C for 8 h.

Characterization. The crystal phase and purity of the product were characterized by X-ray powder diffraction. Before XRD analysis, electrodeposited powder were firstly striped from nickel foam, checked by magnet to prevent the impurity of nickel and then ultrasonicated for 60 min. X-ray diffraction (XRD) data of samples were collected with a D8 Bruker Advance X-ray diffractometer, using Cu Kα radiation (γ = 1.5418 Å) in a 2θ range from 10° to 80° at room temperature. Atomic Adsorption Spectrum was charaterized by GBC (Australia). Scanning electron microscope (SEM) performed on JEOL-7100F was used to characterize the morphology of the synthesized nanomaterials. Transmission electron microscopic (TEM), high-resolution TEM images were recorded by using a JEOL JEM-2010 FEF microscope at an accelerating voltage of 200 kV.

Electrochemical measurement. A three electrodes method consisting of nickel foam as working electrode (typically 1 cm^2), Pt wire and Ag/AgCl (saturated KCl) electrodes as counter and reference electrodes were used. Cyclic voltammetry and galvanostatic charge–discharge studies were performed using an Autolab Potentiostat Galvanostat. Na$_2$SO$_4$ (1 M) solution was used as the electrolyte for all the electrochemical test. To compare the electrochemical behaviors of Na$_x$MnO$_2$/MnO$_2$ with those of Li$_x$Mn$_2$O$_4$/MnO$_2$ in Na$^+$ or Li$^+$ electrolytic system and further illustrate our advantages of pre- intercalation, Li$_2$SO$_4$ (1 M) solution was also used. All electrodeposited electrodes with free-standing Na$_x$MnO$_2$/MnO$_2$ nanoflakes or Li$_x$Mn$_2$O$_4$/MnO$_2$ were well rinsed by deionized water, and then set as working electrode. For the hydrothermally synthesized α-MnO$_2$, the working electrode was consisted of 60 wt% of the active material, 35.5 wt% of conductivity agent (carbon black, Super-P-Li) and 4.5 wt% of binder (polytetrafluoroethylene).

1. Conway, B. E. Electrochemical Supercapacitors: Scientific Fundamentals and Technological Applications. (Springer; 1999).
2. Winter, M. & Brodd, R. J. What are batteries, fuel cells, and supercapacitors? *Chem. Rev.* **104**, 4245–4269 (2004).
3. Simon, P. & Gogotsi, Y. Materials for electrochemical capacitors. *Nature Mater.* **7**, 845–854 (2008).
4. Aricò, A. S., Bruce, P., Scrosati, B., Tarascon, J. M. & Van Schalkwijk, W. Nanostructured materials for advanced energy conversion and storage devices. *Nature Mater.* **4**, 366–377 (2005).
5. Miller, J. R. & Simon, P. Electrochemical capacitors for energy management. *Science* **321**, 651–652 (2008).
6. Pech, D. *et al.* Ultrahigh-power micrometer-sized supercapacitors based on onion-like carbon. *Nature Nanotech.* **5**, 651–654 (2010).
7. Chmiola, J., Largeot, C., Taberna, P. L., Simon, P. & Gogotsi, Y. Monolithic Carbide-derived carbon films for micro-supercapacitors. *Science* **328**, 480–483 (2010).
8. Huang, J. S., Sumpter, B. G. & Meunier, V. Theoretical model for nanoporous carbon supercapacitors. *Angew. Chem. Int. Ed.* **47**, 520–524 (2008).
9. Lee, S. W., Gallant, B. M., Byon, H. R., Hammond, P. T. & Shao-Horn, Y. Nanostructured carbon-based electrodes: bridging the gap between thin-film lithium-ion batteries and electrochemical capacitors. *Energy Environ. Sci.* **4**, 1972–1985 (2011).
10. Chen, W. *et al.* High-Performance Nanostructured Supercapacitors on a Sponge. *Nano Lett.* **11**, 5165–5172 (2011).
11. Pang, S. C. & Anderson, M. A. Novel electrode materials for electrochemical capacitors: Part II. Material characterization of sol-gel-derived and electrodeposited manganese dioxide thin films. *J. Mater. Res.* **15**, 2096–2106 (2000).
12. Chang, J. K. & Tsai, W. T. Material characterization and electrochemical performance of hydrous manganese oxide electrodes for use in electrochemical pseudocapacitors. *J. Electrochem. Soc.* **150**, A1333–A1338 (2003).
13. Be'langer, D., Brousse, T. & Long, J. W. Manganese oxides: battery materials make the leap to electrochemical capacitors. *Electrochem. Soc. Interface* **17**, 49–52 (2008).
14. Liu, R. & Lee, S. B. MnO$_2$/poly(3,4-ethylenedioxythiophene) coaxial nanowires by one-step coelectrodeposition for electrochemical energy storage. *J. Am. Chem. Soc.* **130**, 2942–2943 (2008).
15. Hu, C.-C., Chang, K.-H., Lin, M.-C. & Wu, Y.-T. Design and tailoring of the nanotubular arrayed architecture of hydrous RuO$_2$ for next generation supercapacitors. *Nano Lett.* **6**, 2690–2695 (2006).
16. Sugimoto, W., Iwata, H., Yasunaga, Y., Murakami, Y. & Takasu, Y. Preparation of ruthenic acid nanosheets and utilization of its interlayer surface for electrochemical energy storage. *Angew. Chem. Int. Ed.* **42**, 4092–4096 (2003).
17. Hu, L. B. *et al.* Symmetrical MnO$_2$-carbon nanotube-textile nanostructures for wearable pseudocapacitors with high mass loading. *Acs Nano* **5**, 8904–8913 (2011).
18. Lee, S. W., Kim, J., Chen, S., Hammond, P. T. & Shao-Horn, Y. Carbon nanotube/manganese oxide ultrathin film electrodes for electrochemical capacitors. *Acs Nano* **4**, 3889–3896 (2010).
19. Zhang, H., Yu, X. & Braun, P. V. Three-dimensional bicontinuous ultrafast-charge and -discharge bulk battery electrodes. *Nature Nanotech.* **6**, 277–281 (2011).
20. Lang, X., Hirata, A., Fujita, T. & Chen, M. Nanoporous metal/oxide hybrid electrodes for electrochemical supercapacitors. *Nature Nanotech.* **6**, 232–236 (2011).
21. Cross, A., Morel, A., Cormie, A., Hollenkamp, T. & Donne, S. Enhanced manganese dioxide supercapacitor electrodes produced by electrodeposition. *J. Power Sources* **196**, 7847–7853 (2011).
22. Toupin, M., Brousse, T. & Bélanger, D. Charge Storage Mechanism of MnO$_2$ electrode used in aqueous electrochemical capacitor. *Chem. Mater.* **16**, 3184–3190 (2004).
23. Mendiboure, A., Delmas, C. & Hagenmuller, P. Electrochemical intercalation and deintercalation of Na$_x$MnO$_2$ bronzes. *J. Solid State Chem.* **57**, 323–331 (1985).
24. Caballero, A. *et al.* Synthesis and characterization of high-temperature hexagonal P2-Na$_{0.6}$MnO$_2$ and its electrochemical behaviour as cathode in sodium cells. *J. Mater. Chem.* **12**, 1142–1147 (2002).
25. Ma, X., Chen, H. & Ceder, G. Electrochemical Properties of Monoclinic NaMnO$_2$. *J. Electrochem. Soc.* **158**, A1307–A1312 (2011).
26. D'Arienzo, M. *et al.* Layered Na$_{0.71}$CoO$_2$: a powerful candidate for viable and high performance Na-batteries. *Phys. Chem. Chem. Phys.* **14**, 5945–5952 (2012).
27. Berthelot, R., Carlier, D. & Delmas, C. Electrochemical investigation of the P2-Na$_x$CoO$_2$ phase diagram. *Nature Mater.* **10**, 74–U73 (2011).
28. Guignard, M. *et al.* P2-NaxVO2 system as electrodes for batteries and electron-correlated materials. *Nature Mater.* **12**, 74–80 (2013).
29. Mai, L. Q. *et al.* Lithiated MoO$_3$ nanobelts with greatly improved performance for lithium batteries. *Adv. Mater.* **19**, 3712–3716 (2007).
30. Lu, W. & Lieber, C. M. Nanoelectronics from the bottom up. *Nature Mater.* **6**, 841–850 (2007).
31. Lieber, C. M. & Wang, Z. L. Functional nanowires. *Mrs Bull.* **32**, 99 (2007).
32. Yang, P. & Tarascon, J. M. Towards systems materials engineering. *Nature Mater.* **11**, 560–563 (2012).
33. Hochbaum, A. I. & Yang, P. Semiconductor nanowires for energy conversion. *Chem. Rev.* **110**, 527 (2010).
34. Yu, P., Zhang, X., Wang, D., Wang, L. & Ma, Y. Shape-controlled synthesis of 3D hierarchical MnO$_2$ nanostructures for electrochemical supercapacitors. *Cryst. Growth Des.* **9**, 528–533 (2009).
35. Devaraj, S. & Munichandraiah, N. Surfactant stabilized nanopetals morphology of α-MnO$_2$ prepared by microemulsion method. *J. Solid State Electrochem.* **12**, 207–211 (2008).
36. Wang, Y. *et al.* Structural-controlled synthesis of manganese oxide nanostructures and their electrochemical properties. *J. Alloys Compd.* **509**, 8306–8312 (2011).
37. Fischer, A. E., Pettigrew, K. A., Rolison, D. R., Stroud, R. M. & Long, J. W. Incorporation of Homogeneous, Nanoscale MnO$_2$ within ultraporous carbon structures via self-limiting electroless deposition: implications for electrochemical capacitors. *Nano Lett.* **7**, 281–286 (2007).
38. Lytle, J. C. *et al.* The right kind of interior for multifunctional electrode architectures: carbon nanofoam papers with aperiodic submicrometre pore networks interconnected in 3D. *Energy Environ. Sci.* **4**, 1913–1925 (2011).
39. Wei, W., Cui, X., Mao, X., Chen, W. & Ivey, D. G. Morphology evolution in anodically electrodeposited manganese oxide nanostructures for electrochemical supercapacitor applications-Effect of supersaturation ratio. *Electrochim. Acta* **56**, 1619–1628 (2011).
40. Babakhani, B. & Ivey, D. G. Effect of electrodeposition conditions on the electrochemical capacitive behavior of synthesized manganese oxide electrodes. *J. Power Sources* **196**, 10762–10774 (2011).
41. Kim, J.-H., Lee, K. H., Overzet, L. J. & Lee, G. S. Synthesis and electrochemical properties of spin-capable carbon nanotube sheet/MnO$_x$ composites for high-performance energy storage devices. *Nano Lett.* **11**, 2611–2617 (2011).
42. Zanello, P. Inorganic Electrochemistry: Theory, Practice and Application (Royal Society of Chemistry; 2003).

43. Bard, A. J. & Faulkner, L. R. Electrochemical Methods: Fundamentals and Applications (Wiley; 2000).

Acknowledgments

Author contributions

H.L., Z.Z., W.K. performed the experiments. L.M., H.L., Y.Z. designed the experiments, discussed the interpretation of results and co-wrote the paper. All authors discussed the results and commented on the manuscript.

Additional information

Supplementary information accompanies this paper at http://www.nature.com/scientificreports

Competing financial interests: The authors declare no competing financial interests.

How to cite this article: Mai, L. *et al.* Fast Ionic Diffusion-Enabled Nanoflake Electrode by Spontaneous Electrochemical Pre-Intercalation for High-Performance Supercapacitor. *Sci. Rep.* **3**, 1718; DOI:10.1038/srep01718 (2013).